Exploring Local Electrostatic Effects with Scanning Probe Microscopy: Implications for Piezoresponse Force Microscopy and Triboelectricity

Nina Balke,* Petro Maksymovych, Stephen Jesse, Ivan I. Kravchenko, Qian Li, and Sergei V. Kalinin

Center for Nanophase Materials Sciences, Oak Ridge National Laboratory, Oak Rige, Tennessee 37831, United States

ABSTRACT The implementation of contact mode Kelvin probe force microscopy (cKPFM) utilizes the electrostatic interactions between tip and sample when the tip and sample are in contact with each other. Surprisingly, the electrostatic forces in contact are large enough to be measured even with tips as stiff as 4.5 N/m. As for traditional noncontact KPFM, the signal depends strongly on electrical properties of the sample, such as the dielectric constant, and the tip properties, such as the stiffness. Since the tip is in contact with the sample, bias-induced changes in the junction potential between tip and sample can be measured with higher lateral and temporal resolution compared to traditional noncontact KPFM. Significant and reproducible variations of tip–surface capacitance are observed and attributed to surface electrochemical phenomena. Observations of significant surface charge states at zero bias and strong hysteretic electromechanical responses at a nonferroelectric surface have significant implications for fields such as triboelectricity and piezoresponse force microscopy.

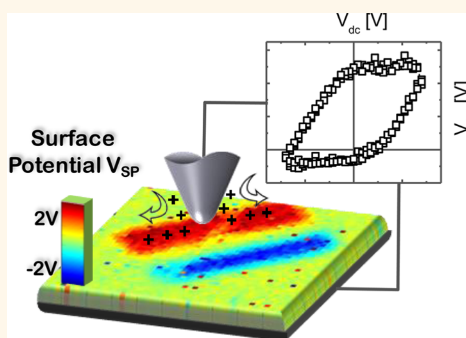

KEYWORDS: scanning probe microscopy · electrostatics · charge storage · HfO_2 · thin films

Kelvin probe force microscopy (KPFM) has been developed to study the contact potential difference (CPD) between an atomic force microscopy tip and the sample surface. This noncontact technique is based on the electrostatic interactions of the AFM tip and the sample.[1] It is routinely used to study surface potentials of solid materials for various applications. The most commonly used operating mode is amplitude-modulated KPFM, where the topography of the studied sample is recorded followed by a second scan line at a certain height above the sample, where the previously recorded sample height is retraced and the CPD between the tip and sample is measured by applying dc (V_{dc}) and ac voltages (V_{ac}) to the tip, and the oscillation of the tip as a function of V_{DC} is analyzed. Therefore, the tip and the surface are always separated by an air or vacuum gap in KPFM and the technique cannot by its very implementation measure the contact potential difference across the junction between two materials (jCPD).

In some cases, CPD and jCPD are the same value. This is the case of metal–metal junctions, for example, if there is no passivating surface layer present. However, for materials that chemically interact when forming a junction, or for charge-induced processes in the junction (ionic motion, charge injection, and electrochemistry), CPD and jCPD are not necessarily the same. Moreover, jCPD values can have very strong time dependence and relax on sub-millisecond time scales as determined by the lifetime and mobility of surface and injected ionic species, lifetimes of trapped charges, *etc.*[2,3] In this case, CPD measured by KPFM will not necessarily represent the true jCPD value, and it can be fundamentally different from it in some cases. Naturally, the sensitivity of electrostatic probes to local chemistry also raises a possibility of detecting junction electrochemical effects that are missed by KPFM. One other major limitation of KPFM is poor spatial resolution (compared to other AFM-based techniques) and the inability to study fast charge dissipation and detrapping

* Address correspondence to balken@ornl.gov.

Received for review June 20, 2014 and accepted September 25, 2014.

Published online September 25, 2014
10.1021/nn505176a

© 2014 American Chemical Society

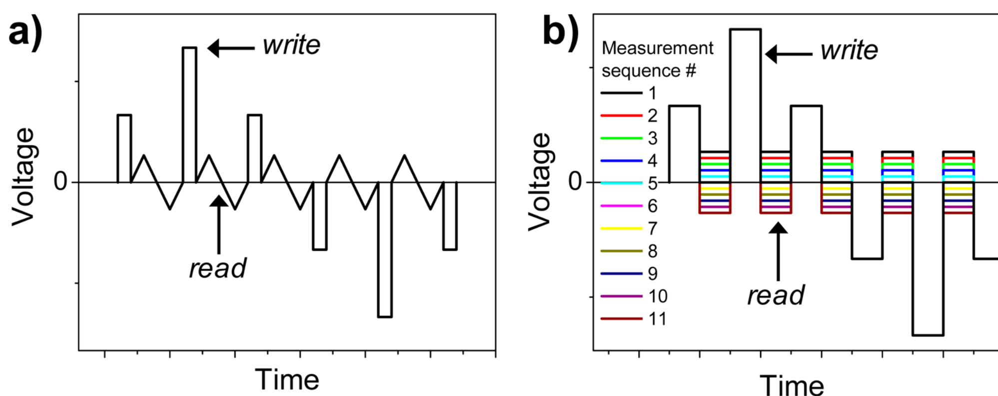

Figure 1. Experimental biasing schemes for V_{dc} to perform open-loop KPFM through a voltage sweep after dc voltage pulses (a) and through stepwise increase of read voltage after the voltage pulse in sequential measurements (b). The ac voltages are superimposed on the shown voltage sequences.

processes in nonmetallic materials. Dual-frequency techniques have been implemented to address the long scan times,[4,5] but an improvement of existing techniques is needed to address the remaining problems of lateral and time resolution.

Electrostatic forces acting between the tip and the sample also exist when the tip is in physical contact with the sample surface. As for KPFM, in contact Kelvin probe force microscopy (cKPFM) a dc and ac voltage are applied to the tip, whereas the frequency of the ac voltage is chosen to be close to the (contact) resonance frequency or consist of a band of frequencies around the contact resonance frequency.[6] The concept of detecting electrostatic forces between the tip and sample in contact has been utilized in the past in form of contact electrostatic force microscopy (EFM).[7,8] All measurement schemes typically implemented for KPFM, such as open-loop or closed-loop KPFM,[4,9−12] and principles of data analysis can also be applied for cKPFM, which makes it easy to adapt this technique in existing SPMs.

Here, we utilize open-loop cKPFM because a non-optimized V_{dc} feedback can result in additional and unwanted charge injection if feedback instability leads to large excursion of compensating potential. In order to investigate charge injection and charge trapping, dc voltage pulses are applied to the tip in contact with an amorphous HfO_2 thin film. Previously, charge storage in HfO_2 has been investigated macroscopically with top electrodes.[13,14] However, macroscopic device characterization averages over length scales much larger than the basic atomic processes of charge injection. Therefore, it is beneficial to develop a technique with higher temporal and spatial resolution to be able to study charge transfer between metal and dielectric materials, which is a key component in processes such as flash memories,[15] electroforming in memristors,[16] surface electrochemistry,[17] and triboelectricity.[18]

RESULTS AND DISCUSSION

To measure the junction potential after each pulse, two measurement schemes are used. The first is shown in Figure 1a and consists of a small-amplitude dc voltage sweep after each voltage pulse (read step). The measured tip oscillation during the voltage sweep can be used to extract the junction potential without any additional feedback (open-loop cKPFM). The drawback for this approach is the time it takes to sweep the voltage, which excludes the tracking of fast potential changes. To overcome this, multiple cycles of dc voltage pulses can be applied subsequently with varying dc voltage read steps as outlined in Figure 1b. The read step can be of very short duration, enabling tracking fast charge injection and dissipation processes. However, this method can only be applied if the observed phenomena are independent of the measurement history, *i.e.*, the voltage-induced material changes have fast relaxation times and are completely reversible.

To demonstrate the principle of cKPFM and compare it to KPFM, charge patterns were written by applying ±5 V to a scanning tip under a 45 deg scan angle in a 10 nm thick HfO_2 film grown on Si. The measured surface potential from closed-loop KPFM and a representative section of the image are shown in Figure 2a and b, respectively. In the area where −5 V was applied the surface potential was reduced from 0.4 V to −0.11 V, and in the area with 5 V writing voltage the surface potential was increased to 1.05 V. In the same area, cKPFM (open loop) was performed according to the experiment outlined in Figure 1a. The cKPFM signal changes linearly with V_{dc} and the junction potential is extracted through the *x*-intercept of a linear fit through the data, *i.e.*, tip potential corresponding to the zero first harmonic of the force.

The resulting map of the junction potential is shown in Figure 2c, in which the written charge pattern is clearly visible. Figure 2d shows the average of 10 curves from the red and blue area in Figure 2c. The values for the junction potential are close to those measured with KPFM, but with slightly larger magnitudes. This can be explained by a higher lateral resolution in the contact mode compared with KPFM, which scales with the lift scan height and the cantilever dimensions. To compare

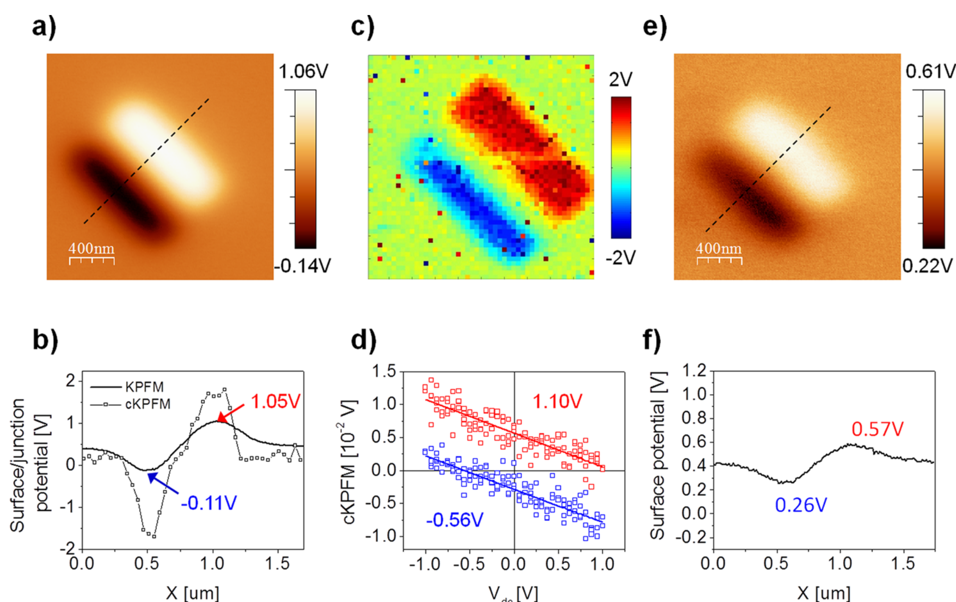

Figure 2. Surface potential map from KPFM measurement after charge injection with ±5 V applied to the scanning tip (a) with selected cross section (b). Junction potential map from open-loop cKPFM measurement performed after KPFM (c) and averaged cKPFM curves from the two different areas (d). A cross section of the data in (c) is displayed in (b) for comparison. Surface potential map from KPFM measurement after cKPFM experiment (e) with selected cross section (f).

the lateral resolution of KPFM and cKPFM, a cross section of Figure 2c is plotted in Figure 2b together with the cross section of the KPFM measurement. It can be seen that the areas are better defined and the peaks are narrower for cKPFM due to the improved lateral resolution.

While the charges on the sample surface can be easily detected, their nature is unknown. The observed charges can be physical, chemical, or electrochemical in origin. Physical charges can be described as charge injection into existing traps, chemical charges can be described by the electromigration of ions on the surface or bulk, while electrochemical charges can be described through the formation of traps followed by charge trapping. The same is true for the detrapping process. At this point, we cannot differentiate between these scenarios, although studies with varying electrochemical potential of volatile species can provide additional control on the electrochemical phenomena. After cKPFM, traditional KPFM was repeated, and it was observed that the surface potentials were strongly reduced.

To investigate the dissipation of charges, multiple KPFM images were measured after writing the charge pattern as shown in Figure 3a. Every image took about 6 min; that is, the charges were stable over at least 30 min, which is also visible in the extracted line scans as a function of scan number in Figure 3c. To improve the speed of the cKPFM images, only V_{ac} is applied during scanning after charge writing. This is equivalent to measuring the *y*-intercept of the cKPFM curves at $V_{dc} = 0$ (Figure 2d), which is analogous to EFM in contact mode (cEFM). From this signal, jCPD can be calculated if the slopes of the cKPFM curves are constant and independent of the junction potential. Later, we show that the dynamics are more complex (this assumption is not verified) and that the change in slope will give access to more system information such as capacitance gradient and contact stiffness.

The image series in Figure 3b shows the quick dissipation of charges when scanned in contact. The first image in Figure 3b clearly shows the two differently charged regions. The area written with −5 V appears with a high negative value, whereas the region written with +5 V appears as a high positive value. This is due to the fact that the *y*-intercept is changing from negative to positive when positive or negative charges are injected, respectively, which is also visible in Figure 2d. The fast dissipation of charges is very clear when looking at line scans through the images (Figure 3d). Every image was recorded within 3 min; that is, the charges dissipated completely within 6 min. The strong difference in charge dissipation when the tip is not in contact or in contact with the surface demonstrates the role of a local gate electrode, which assists in the charge detrapping. Alternatively, charges generated through friction when the tip scans over the surface can play a role in the dissipation process. When the first images in Figure 3a and b are compared, it can be seen that the contact version of KPFM yields higher spatial resolutions, as seen from the sharpness of contrast between differently charged areas. At this point, we want to emphasize that cEFM and piezoresponse force microscopy (PFM) are identical in terms of bias application and signal detection. Therefore, when PFM is performed on HfO_2, the resulting image would be identical to the first image in Figure 3b. Such a contrast in PFM images can be interpreted as the existence of ferroelectric domains, and ferroelectric

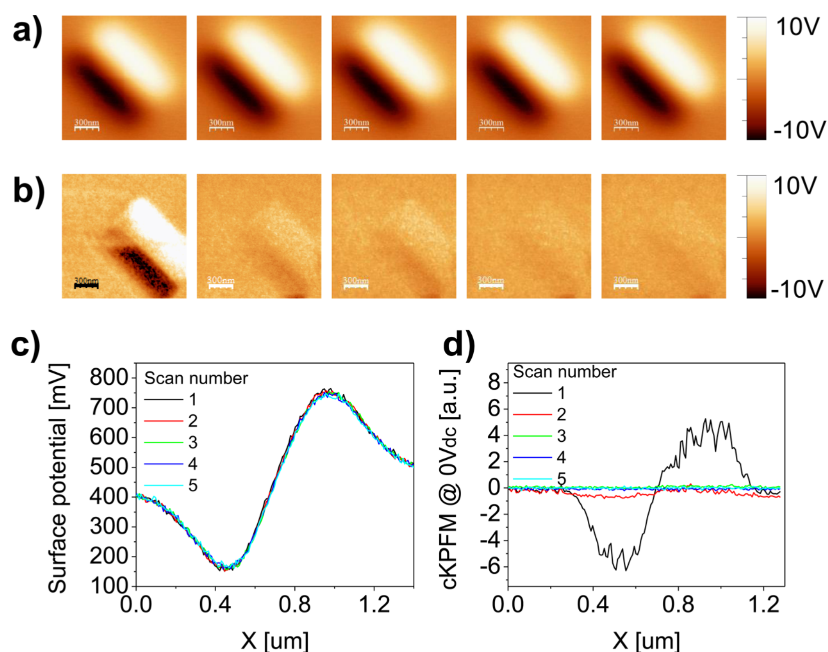

Figure 3. Five subsequent scan surface potential images for KPFM (a) and junction potential images from cKPFM (0 V_{dc}) maps (b) after charge writing with ±5 V applied to the scanning tip and corresponding cross sections (c, d).

material properties can be concluded. However, this interpretation would be false since the existence of surface charges alone can explain the observed contrast. The same is true for the technique of electrochemical strain microscopy (ESM), which is used to study the volume changes caused by locally induced changes in ionic concentration in ionic conductors.[19,20] The contribution of surface charges to the measured ESM signal needs to be critically studied.

The detrapping of charges through the presence of the SPM tip in contact with the sample is further illustrated by Figure 4. A charge pattern was written with a scanning SPM tip (Figure 4a), and the topography (Figure 4b) together with EFM amplitude and phase images (Figure 4c and d) were recorded. During EFM, only V_{ac} voltages are applied to the tip in a certain height over the sample and the electrostatic forces are measured as change in amplitude and phase of the cantilever oscillation. The charged regions can easily be identified by the topography image, which shows features between 1 and 2 nm high. They can be seen only when imaged in noncontact (tapping) mode but not in contact mode. That means the topography change is just a measurement artifact due to strong electrostatic tip–sample interactions, or it is not stable when imaged in contact mode. It is also interesting to note that even the regions where 0 V_{dc} was applied during the charge writing process (see Figure 4a) are visible in the topography and EFM images. This could be an effect of tribologic surface charging or removal of passivating surface layers with the tip.

After the EFM images were recorded, a central section was scanned with the SPM tip at 0 V_{dc} in contact mode (Figure 4e). This led to a removal of the surface charges as visible in Figure 4f–h. Similar experiments have been performed on ferroelectric materials,[21] where changes in ferroelectric domains were investigated after mechanical force exerted by the SPM using PFM. Due to the above-mentioned cross-correlation between PFM and cEFM, changes in junction potentials after an SPM tip in contact with the sample as demonstrated in Figure 4 could appear as changes in PFM images. This cross-talk between surface charges and PFM signals needs to be considered when interpreting PFM images and *vice versa*.

The higher spatial resolution of cKPFM as follows from localized detection of electrostatic forces allows high-accuracy studies of local relaxation. Positive or negative voltage pulses were applied to the tip in contact with the tip, and the relaxation of the junction potential was recorded with open-loop cKPFM according to Figure 1a and open-loop KPFM as a function of time. The curves were linearly fitted and the junction potential was extracted through the *x*-axis intercept. Figure 5a shows the comparison of the two methods. It can be seen from the cKPFM measurement that the junction potential is enhanced and reduced after positive and negative voltage pulses, respectively, and relaxes back to one common potential around 0.75 V within 300 s. In comparison, the surface potential measured by noncontact KPFM does not show any changes in surface potential after the two different voltage pulses. This fact can be explained by the small area underneath the tip, which was affected by the voltage pulse and the poor lateral resolution of KPFM, which is due to the global signal contribution from the whole cantilever. This demonstrates that electrostatic forces are acting locally on the tip cone, therefore

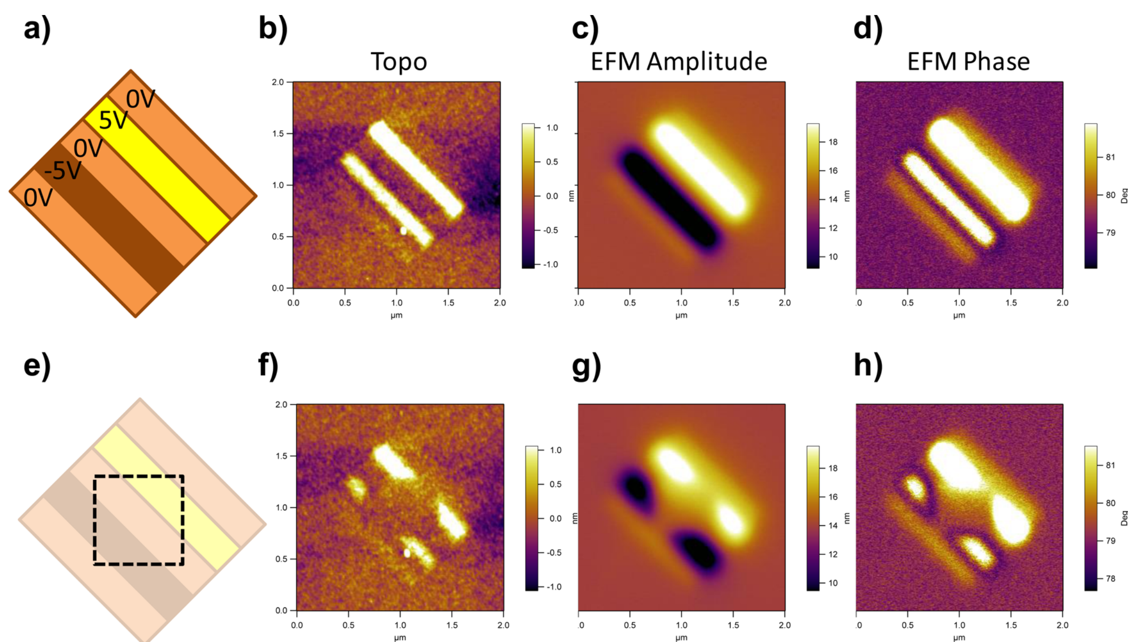

Figure 4. Charge writing pattern (a), topography measured in noncontact mode (b) and EFM amplitude (c) and phase (d). Second scan area with 0 V_{dc} performed in contact mode (e), followed by measurement of topography measured in noncontact mode (f) and EFM amplitude (g) and phase (h).

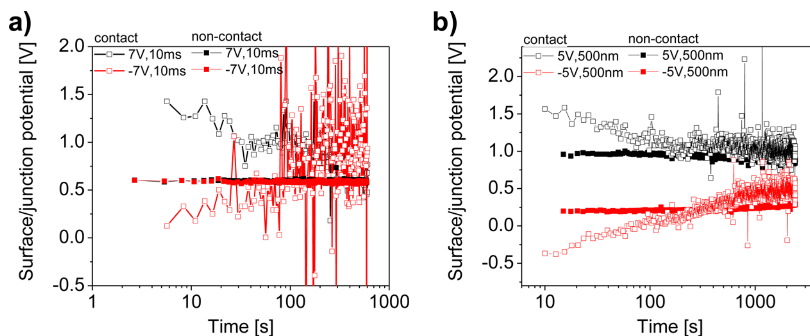

Figure 5. Comparison of junction potential relaxation recorded with KPFM and open-loop cKPFM for a single point (a) and a 500 nm by 500 nm area (b).

improving the lateral resolution in contact mode. On the other hand, the cKPFM data have a lower signal/noise ratio compared with KPFM, which results in unfeasible fits to extract the junction potential, which can be seen in Figure 5a for long relaxation times when the junction potential becomes very small.

In order to see the changes in surface potential using KPFM, charges needed to be injected in larger areas to compensate for lower spatial resolution. This was accomplished by scanning a 500 nm by 500 nm area with an applied voltage as shown in Figure 5b. Here, the KPFM data show a clearly different surface potential around the original surface potential. However, no relaxation over time can be observed. For the cKPFM measurement, the initial junction potential is larger than measured by KPFM but then relaxes within 300 s to the KPFM values and slightly below afterward. This fits well with the observations described in Figures 3 and 4.

We further explore the measurement of junction potentials with a different measurement scheme (Figure 1b). Depending on the technical implementation of the open-loop cKPFM measurement, it can take between 1 and 10 s to get the first data point after changing the junction potential. In order to access lower time scales, the measurement scheme introduced in Figure 1b is investigated. This is analogous to a spectroscopic measurement where the voltage of the read step is changed in subsequent cycles. This spectroscopic cKPFM approach is valid only if the induced changes in surface/junction potentials are reversible and the measurement history does not influence the future measurements. This has been validated for our measurement. Figure 6a shows the measured cKPFM signal as a function of the voltage during the read step, V_{read}, after voltage pulses between $+7$ and -7 V. It can be seen that the curves are always linear but show different offsets after the applied voltage pulses. From these, the junction potential can be extracted, which is shown in Figure 6b. The junction potential changes hysteretically when the pulse

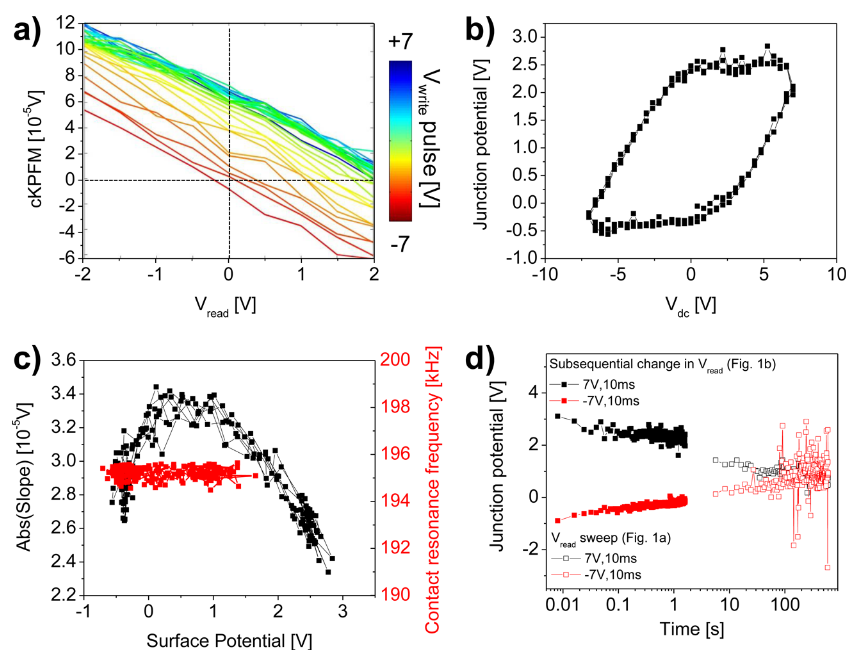

Figure 6. cKPFM as a function of V_{read} after different voltage pulses (a). Extracted junction potential as a function of voltage pulse (b). Slope of curves in (a) and contact resonance frequency measured by AFAM as a function of junction potential (c). Relaxation of junction potential measured with two different measurement schemes from Figure 1d.

voltage is swept between +7 and −7 V. In the beginning, the junction potential is close to zero and becomes more positive with positive voltages applied to the tip and more negative with negative voltages applied to the tip. The hysteresis can be explained by dynamic changes in surface charge from the tip, charge trapping, and detrapping. These charges can be physical, chemical, or electrochemical in nature, and we do not distinguish between them.

A peculiar property of the slope of the curves shown in Figure 6a is a slight change of the slope magnitude during the measurement and a strong correlation to the measured junction potential (Figure 6c). This shows that it is not enough to measure the *y*-intercept of the open-loop cKPFM curve to extract the junction potential, and we get more information about the system by performing cKPFM without closed-loop feedback. Since the curves in Figure 6a are determined by electrostatic interactions, the slope is proportional to the capacitance gradient and the stiffness of the tip—sample contact as in regular KPFM. Additional forces on the tip through the presence of the surface charges injected by the tip could change the contact stiffness, which is proportional to the contact resonance frequency, f_c. In order to measure if f_c changes as a function of potential, atomic force acoustic microscopy (AFAM)[22,23] was performed. Here, the dc voltage pulses were applied to the tip, whereas ac voltages were used to oscillate the sample mechanically; that is, the tip oscillations are not driven electrostatically as in the previous experiments. In Figure 6c, the change of contact resonance frequency as a function of junction potential is displayed for a different location. No changes in f_c can be detected. Therefore, the changes in slope of cKPFM curves can be attributed to the change in capacitance gradient, which scales with the presence of surface charges. This could be due to changes in chemical capacitance formed by electric double layers in the bulk or on the sample surface and is subject to further studies.

The same measurement scheme can be applied to look at the charge relaxation after a single voltage pulse, as done in Figure 5a. The comparison of the two measurement schemes in Figure 1 applied to look at charge relaxation is shown in Figure 6d. The measurement scheme from Figure 1b allows us to access time scales down to 4 ms and up to around 1 s and lines up nicely with the result shown in Figure 5a at larger time scales. This demonstrates the reversible charge trapping and detrapping process, which is necessary to apply the experimental scheme depicted in Figure 1b and the improved temporal resolution of cKPFM when operated in a spectroscopic mode.

CONCLUSIONS

We implemented cKPFM to study junction potentials in heterojunctions between metals and dielectric materials. KPFM in contact mode allows for higher spatial and temporal resolution compared to traditional KPFM and enables access to additional physical phenomena such as charge detrapping and changes in contact properties through electrostatic interactions between the tip and sample. We demonstrated the technique by studying charge trapping and detrapping in amorphous HfO_2 thin films and found strong charge detrapping assisted by the presence of the SPM tip.

The findings using cKPFM also apply to similar SPM-based measurement techniques, *e.g.*, PFM. The similarity between cKPFM and PFM methods can result in misinterpretation of data on supposedly ferroelectric samples which originate from changes in junction potentials through charge injection and charge relaxation. The hysteretic changes in the *y*-axis intercept in Figure 6a after different voltage pulses would appear as a hysteretic PFM loop that shows phase flips and amplitude saturation, which is presently used to establish the ferroelectric nature of a material. When PFM is performed on the HfO_2 samples, the resulting PFM hysteresis loop is absolutely identical to the change in *y*-intercept after a change in junction potential. It has been discussed and predicted that HfO_2 can become ferroelectric under certain circumstances,[24−28] which is not the case for the amorphous HfO_2 sample studied here.

In the future, cKPFM can be used to study physical, chemical, and electrochemical processes in the tip−sample junction on a variety of materials. To achieve this, environmental and chemistry controls may become necessary to differentiate between these processes. In addition, cKPFM can be used to study triboelectricity or help identify signal origins in other SPM-type experiments by combining them with cKPFM.

METHODS

Experimental Section. KPFM and cKPFM were measured on commercial SPM systems in a glovebox environment to reduce the role of surface water layers (Bruker Icon). EFM measurements were performed in ambient environment (Asylum Research Cypher). All SPMs are equipped with external data-acquisition electronics based on an NI-6115 fast DAQ card to generate the probing signal and store local hysteresis loops and correlate them with surface topography. The AFM tip had a nominal stiffness of about 2.8 N/m and was conductively coated with Pt/Ir (Nanosensor) to apply the local bias to the sample. For all measurements, band excitation techniques[6] are used and the measured contact resonance peaks are fitted to a simple harmonic oscillator to extract the surface oscillation. The AFAM measurements were performed using an acoustic sample stage (Asylum Research, MFP-3D).

Sample Preparation. Amorphous 10 nm HfO_2 layers were grown on Si(100) 4 in. wafers using an Oxford Instruments FlexAl atomic layer deposition (ALD) system. Liquid tetrakis-(ethylmethylamino)hafnium (TEMAH) purchased from Air Liquide was the hafnium precursor. A standard Oxford plasma process was utilized, and O_2 gas was used as an oxidant. The wafer substrate temperature during the process was kept at 563 K. Argon gas was the carrier gas for both TEMAH and O_2. The chamber pressure during the precursor and oxidation steps was 10.7 and 2 Pa, respectively. The growth rate was estimated at 0.0997 nm per cycle. Native silicon oxide was not removed from the wafer surface before deposition.

Conflict of Interest: The authors declare no competing financial interest.

Acknowledgment. Personal support was provided by the U.S. Department of Energy, Basic Energy Sciences, Materials Sciences and Engineering Division, through the Office of Science Early Career Research Program (N.B., Q.L.).The experiments were performed at the Center for Nanophase Materials Sciences, which is sponsored at Oak Ridge National Laboratory by the Scientific User Facilities Division, Office of Basic Energy Sciences, U.S. Department of Energy, which also provided personal support (P.M., S.J., I.I.K., S.V.K.).

REFERENCES AND NOTES

1. Sadewasser, S.; Glatzel, T. *Kelvin Probe Force Microscopy*; Springer: Berlin, 2012.
2. Johnson, J. P.; Winslow, D. W.; Williams, C. C. Measurement of Depth and Energy of Buried Trap States in Dielectric Films by Single Electron Tunneling Force Spectroscopy. *Appl. Phys. Lett.* **2011**, *98*, 052902.
3. Johnson, J. P.; Zheng, N.; Williams, C. C. Atomic Scale Imaging and Spectroscopy of Individual Electron Trap States Using Force Detected Dynamic Tunnelling. *Nanotechnology* **2009**, *20*, 055701.
4. Collins, L.; Kilpatrick, J. I.; Weber, S. A. L.; Tselev, A.; Vlassiouk, I. V.; Ivanov, I. N.; Jesse, S.; Kalinin, S. V.; Rodriguez, B. J. Open Loop Kelvin Probe Force Microscopy with Single and Multi-Frequency Excitation. *Nanotechnology* **2013**, *24*, 475702.
5. Ding, X. D.; Li, C.; Liang, Z. W.; Lin, G. C., Resonant Multi-Frequency Method for Kelvin Probe Force Microscopy in Air. *Meas. Sci. Technol.* **2012**, *23*.
6. Jesse, S.; Kalinin, S. V.; Proksch, R.; Baddorf, A. P.; Rodriguez, B. J. The Band Excitation Method in Scanning Probe Microscopy for Rapid Mapping of Energy Dissipation on the Nanoscale. *Nanotechnology* **2007**, *18*, 435503.
7. Johann, F.; Hoffmann, A.; Soergel, E. Impact of Electrostatic Forces in Contact-Mode Scanning Force Microscopy. *Phys. Rev. B* **2010**, *81*, 094109.
8. Hong, J. W.; Park, S. I.; Khim, Z. G. Measurement of Hardness, Surface Potential, and Charge Distribution with Dynamic Contact Mode Electrostatic Force Microscope. *Rev. Sci. Instrum.* **1999**, *70*, 1735–1739.
9. Guo, S. L.; Kalinin, S. V.; Jesse, S. Open-Loop Band Excitation Kelvin Probe Force Microscopy. *Nanotechnology* **2012**, *23*, 125704.
10. Takeuchi, O.; Ohrai, Y.; Yoshida, S.; Shigekawa, H. Kelvin Probe Force Microscopy without Bias-Voltage Feedback. *Jpn. J. Appl. Phys. 1* **2007**, *46*, 5626–5630.
11. Coffey, D. C.; Ginger, D. S. Time-Resolved Electrostatic Force Microscopy of Polymer Solar Cells. *Nat. Mater.* **2006**, *5*, 735–740.
12. Bayerl, D. J.; Wang, X. D. Three-Dimensional Kelvin Probe Microscopy for Characterizing in-Plane Piezoelectric Potential of Laterally Deflected ZnO Micro-/Nanowires. *Adv. Funct. Mater.* **2012**, *22*, 652–660.
13. Gusev, E. P.; D'Emic, C. P. Charge Detrapping in HfO_2 High-Kappa Gate Dielectric Stacks. *Appl. Phys. Lett.* **2003**, *83*, 5223–5225.
14. Zhu, W. J.; Ma, T. P.; Zafar, S.; Tamagawa, T. Charge Trapping in Ultrathin Hafnium Oxide. *IEEE Electron Device Lett.* **2002**, *23*, 597–599.
15. Waser, R.; Aono, M. Nanoionics-Based Resistive Switching Memories. *Nat. Mater.* **2007**, *6*, 833–840.
16. Yang, J. J.; Miao, F.; Pickett, M. D.; Ohlberg, D. A. A.; Stewart, D. R.; Lau, C. N.; Williams, R. S. The Mechanism of Electroforming of Metal Oxide Memristive Switches. *Nanotechnology* **2009**, *20*, 215201.
17. Bockris, J. O. M.; Khan, S. U. *Surface Electrochemistry: A Molecular Level Approache*; Springer: Berlin, 1993.
18. Fan, F. R.; Tian, Z. Q.; Wang, Z. L. Flexible Triboelectric Generator!. *Nano Energy* **2012**, *1*, 328–334.
19. Balke, N.; Jesse, S.; Morozovska, A. N.; Eliseev, E.; Chung, D. W.; Kim, Y.; Adamczyk, L.; Garcia, R. E.; Dudney, N.; Kalinin, S. V. Nanoscale Mapping of Ion Diffusion in a Lithium-Ion Battery Cathode. *Nat. Nanotechnol.* **2010**, *5*, 749–754.

20. Kumar, A.; Ciucci, F.; Morozovska, A. N.; Kalinin, S. V.; Jesse, S. Measuring Oxygen Reduction/Evolution Reactions on the Nanoscale. *Nat. Chem.* **2011**, *3*, 707–713.
21. Lu, H.; Bark, C. W.; de los Ojos, D. E.; Alcala, J.; Eom, C. B.; Catalan, G.; Gruverman, A. Mechanical Writing of Ferroelectric Polarization. *Science* **2012**, *336*, 59–61.
22. Rabe, U.; Amelio, S.; Kester, E.; Scherer, V.; Hirsekorn, S.; Arnold, W. Quantitative Determination of Contact Stiffness Using Atomic Force Acoustic Microscopy. *Ultrasonics* **2000**, *38*, 430–437.
23. Rabe, U.; Arnold, W. Acoustic Microscopy by Atomic-Force Microscopy. *Appl. Phys. Lett.* **1994**, *64*, 1493–1495.
24. Clima, S.; Wouters, D. J.; Adelmann, C.; Schenk, T.; Schroeder, U.; Jurczak, M.; Pourtois, G. Identification of the Ferroelectric Switching Process and Dopant-Dependent Switching Properties in Orthorhombic HfO_2: A First Principles Insight. *Appl. Phys. Lett.* **2014**, *104*.
25. Zhou, D. Y.; Xu, J.; Li, Q.; Guan, Y.; Cao, F.; Dong, X. L.; Muller, J.; Schenk, T.; Schroder, U. Wake-up Effects in Si-Doped Hafnium Oxide Ferroelectric Thin Films. *Appl. Phys. Lett.* **2013**, *103*, 192904.
26. Mueller, S.; Mueller, J.; Singh, A.; Riedel, S.; Sundqvist, J.; Schroeder, U.; Mikolajick, T. Incipient Ferroelectricity in Al-Doped HfO_2 Thin Films. *Adv. Funct. Mater.* **2012**, *22*, 2412–2417.
27. Muller, J.; Schroder, U.; Boscke, T. S.; Muller, I.; Bottger, U.; Wilde, L.; Sundqvist, J.; Lemberger, M.; Kucher, P.; Mikolajick, T., *et al*. Ferroelectricity in Yttrium-Doped Hafnium Oxide. *J. Appl. Phys.* **2011**, *110*, 114113.
28. Muller, J.; Boscke, T. S.; Schroder, U.; Mueller, S.; Brauhaus, D.; Bottger, U.; Frey, L.; Mikolajick, T. Ferroelectricity in Simple Binary ZrO_2 and HfO_2. *Nano Lett.* **2012**, *12*, 4318–4323.